

# RSC Advances



This is an *Accepted Manuscript*, which has been through the Royal Society of Chemistry peer review process and has been accepted for publication.

*Accepted Manuscripts* are published online shortly after acceptance, before technical editing, formatting and proof reading. Using this free service, authors can make their results available to the community, in citable form, before we publish the edited article. This *Accepted Manuscript* will be replaced by the edited, formatted and paginated article as soon as this is available.

You can find more information about *Accepted Manuscripts* in the [Information for Authors](#).

Please note that technical editing may introduce minor changes to the text and/or graphics, which may alter content. The journal's standard [Terms & Conditions](#) and the [Ethical guidelines](#) still apply. In no event shall the Royal Society of Chemistry be held responsible for any errors or omissions in this *Accepted Manuscript* or any consequences arising from the use of any information it contains.



Esterified cellulose nanocrystals were manufactured via one-pot tandem reactions with DMAP as catalyst, during the process cellulose nanocrystallization and acetylation occurred simultaneously.

...



Journal Name

ARTICLE

## One-pot tandem reactions for esterified cellulose nanocrystals preparation with 4-dimethylaminopyridine as catalyst

Qi-lin Lu, Xian-yan Li, Li-rong Tang, Bei-li Lu,\* and Biao Huang\*

Received 00th January 20xx,  
Accepted 00th January 20xx

DOI: 10.1039/x0xx00000x

[www.rsc.org/](http://www.rsc.org/)

An efficient approach for the manufacture of esterified cellulose nanocrystals (E-CNC) via one-pot tandem reactions with 4-dimethylaminopyridine (DMAP) as catalyst under mild operating conditions was put forward. The effects of ball milling time, reaction temperature and ultrasonication time on the yield and degree of substitution (DS) were explored. Characterization indicated the successful esterification of hydroxyl groups of cellulose. Micromorphology and microstructure of the prepared E-CNC were studied using scanning electron microscopy (SEM) and transmission electron microscopy (TEM). Results showed that E-CNC were short rod-like particles with 130-230 nm in length and 20-40 nm in width, forming an interconnected network structure. X-ray diffraction (XRD) results indicated that the crystallinity index increased from 63.5% to 77.2%. The thermal properties of E-CNC were investigated by thermogravimetric analysis (TGA) and the result showed that E-CNC exhibited higher thermal stability compared to that of cellulose pulp.

### 1. Introduction

Cellulose nanocrystals (CNC) have been used as reinforcements in polymers due to their high tensile strength, high flexibility and good dynamic mechanical properties.<sup>1</sup> However, as for the highly polar CNC, the main challenge is related to their uniform dispersion in non-aqueous mediums or in polymeric matrix, and the difficulty in incorporating them into the most common apolar polymers.<sup>2</sup> In order to improve the dispersion, the surface characteristics of CNC must be changed from hydrophilic to more hydrophobic. Acetylation is an efficient chemical modification of the hydroxyl groups on the cellulose, resulting in more hydrophobic surface of cellulose. The earlier reported studies on surface-modified cellulose nanofibers have focused on modification of isolated nanofibers, which usually involved fussy and time-consuming multi-step synthetic protocols.<sup>3</sup>

Nowadays, one-pot reactions have become one of the most attractive synthetic methodologies for reasons of their energy efficiency and general environmental friendliness.<sup>4</sup> One-pot reaction process has been proved to have several advantages over step-wise operations, as it avoids the isolation of intermediate species, thereby considerably reducing the waste generation, increasing efficiency and minimizing the use of solvents, reagents, time and energy.<sup>5</sup> Moreover, it was also found that in most cases the overall yields of one-pot process were usually higher than those obtained from the corresponding step-wise operations. Since the middle of the 1960s, 4-dimethylaminopyridine (DMAP) has been widely used

in many organic synthesis as the catalyst, for example, in the Michael-addition, aldol reactions and esterification reactions.<sup>6</sup> Attracted to the efficiency of the organo-catalyst and the advantage of using water as solvent, we choose DMAP as the catalyst in this work.

Mechanochemistry combines mechanical phenomena and chemical phenomena on a molecular scale, involving phase transition, size reduction and polymer degradation with the effects of compression and friction, cavitation-related phenomena.<sup>9</sup> The size reduction of the solid and accretion of its specific surface area during mechanical milling are accompanied by chemical bonds distorting and bond length extending due to the imposed stress, and when the imposed stress is beyond the chemical bonding energy, bond rupture occurs, which activates effectively the functional chemical groups.<sup>10</sup> Therefore, the mechanochemistry technique would be a potential method to manufacture surface-modified cellulose fillers under mild conditions.

Herein, we gain deeper insight into the efficiency of nanocrystallization and acetylation of cellulose, in particular, disclosing a convenient and versatile method to manufacture functionalized E-CNC in conjunction with ball milling and ultrasonication in tandem mode, in which the nanocrystallization and acetylation of cellulose take place simultaneously. Furthermore, the morphology, structure, spectroscopic and thermal properties of the esterified cellulose nanocrystals are also investigated.

### 2. Experimental

#### 2.1 Materials

Bamboo pulp was supplied by Nanping Paper Co., Ltd (Nanping, Fujian, China), and the acetic acid and

Fujian Agriculture and Forestry University, Fuzhou, China. E-mail: fjhuangbiao@hotmail.com; lubeilihello@gmail.com; Fax: +86 591 83715175; Tel: +86 591 88160598

## ARTICLE

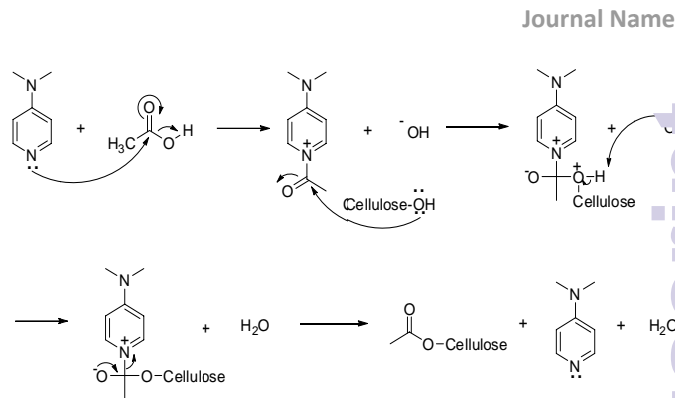
dimethylaminopyridine (DMAP) were purchased from Sinopharm Chemical Reagent Co., Ltd. (Beijing, China). All chemicals used in this work were of analytical grade without any further purification.

## 2.2 Manufacture of esterified cellulose nanocrystals

The bamboo pulp was cut into pieces and beaten to form cellulose pulp with a Fiber Standard Dissociation device (GBT-A, Changchun Yueming Small Testing Machine Co., Ltd., China) for 30 min at 2000 rpm. Mechanochemical pretreatment of cellulose pulp was performed within a planetary ball mill equipped with four agate jars. A mixture of 1 g cellulose pulp, 42 g acetic acid, 0.02 g DMAP and twenty 5-mm agate balls was added into the agate jar and milled at a rotational speed of 500 rpm for 1, 1.5, 2, 2.5 and 3 h, which were labeled as BM (1 h), BM (1.5 h), BM (2 h), BM (2.5 h) and BM (3 h), respectively. After milling, the samples were introduced into a 200 mL two-necked round-bottom flask equipped with a condenser and a polytetrafluoroethylene (PTFE)-coated stirring device and kept at 100-140 °C in an oil bath for 5 h under continuous stirring, followed by an ultrasonication treatment at 20 kHz for 2-4 h in an ultrasonic reactor JY98-IIIN (Ning Bo Scientz Biotechnology Co., Ltd., China). After the reaction, the mixture was washed to neutral with double distilled water by repetitive centrifugations at 10000 rpm for 15 min, and then the esterified cellulose nanocrystals were obtained. A schematic representation of the manufacture of E-CNC is shown in Fig. 1, and the mechanism of the formation of E-CNC is outlined in Scheme 1.



Fig. 1 Schematic model of the manufacture of E-CNC via one-pot tandem reactions.



Scheme 1 Mechanism of the formation of E-CNC with DMAP as catalyst.

## 2.3 Determination of yield and degree of substitution (DS) of E-CNC

The total volume of the manufactured E-CNC suspension was measured. A specified amount of the E-CNC suspension was then transferred to a weighing bottle, followed by freeze-drying. The resulting sample was weighed. The final yield was obtained from the average of three runs of measurements and calculated according to Eq. (1):

$$Y = \frac{(m_1 - m_2)V_1}{m_3V_2} \times 100 \quad (1)$$

Where  $m_1$  is the total mass of dried E-CNC and weighing bottle (mg),  $m_2$  is the mass of the weighing bottle (mg),  $m_3$  is the mass of cellulose pulp (mg),  $V_1$  is the total volume of as-manufactured E-CNC suspension (mL), and  $V_2$  is the volume of E-CNC to be dried (mL).

The degree of substitution of E-CNC was determined by elemental analysis and chemical titration as described previously.<sup>11-12</sup>

## 2.4 Field emission scanning electron microscope (FESEM) examination

The surface morphology of the samples was characterized by means of a XL30 ESEM-FEG model FESEM (FEI Co., Ltd., USA) with an accelerating voltage of 10 kV. All the samples were sputtered and coated with gold before observation.

## 2.5 Transmission electron microscope (TEM) analysis

The microstructure and size of the manufactured esterified cellulose nanocrystals were observed by transmission electron microscope (TEM). Small drops of the E-CNC solution were deposited on a copper grid coated with carbon support film for 1 min, and then the excessive water was drained with filter paper, followed by staining with phosphotungstic acid solution (2 wt%). The grid was dried at room temperature for 12 h, and then analyzed with a JEOL JEM-1010 TEM (Japan Electronics Co., Ltd., Japan) operated at an accelerated voltage of 100 kV.

## 2.6 Fourier-transformed infrared spectra (FTIR) analysis

The chemical structure changes between cellulose pulp and the manufactured esterified cellulose nanocrystals were

analyzed by infrared spectroscopy. FTIR spectra of the samples were obtained with a Nicolet 380 FTIR spectrometer (Thermo Electron Instruments Co., Ltd., USA) in the range of 4000-400  $\text{cm}^{-1}$  with a resolution of 4  $\text{cm}^{-1}$ . Prior to analysis, each sample was first ground into powder, blended with KBr and then pressed into thin pellets.

### 2.7 X-ray photoelectron spectroscopy (XPS) analysis

The chemical compositions of the surface of the esterified cellulose nanocrystals were characterized by X-ray photoelectron spectroscopy. X-ray photoelectron spectrograms were performed using an ESCALAB 250 (Thermo Scientific Instruments Co., Ltd., USA) X-ray Photoelectron Spectrometer equipped with monochromated Al K $\alpha$  X-ray source (1486.6 eV) and operated at a voltage of 15 kV under a current of 10 mA. Elemental surface compositions were determined from low-resolution survey measurements (100 eV pass energy and 1 eV step), and carbon surface chemistry was probed with high resolution regional scans (30 eV pass energy and 0.05 eV step). Surface elemental concentrations and O/C ratios were calculated from the survey spectra. The carbon C1s high-resolution spectra were curve fitted using parameters defined for cellulosic materials and all binding energies were referenced to the aliphatic carbon component of the C1s signal at 285.0 eV.

### 2.8 Solid-state $^{13}\text{C}$ NMR spectroscopy

The NMR experiments were performed with Bruker Avance III 500 spectrometer (Bruker Biospin AG, Fallanden, Switzerland) operated at a  $^{13}\text{C}$  frequency of 125.73 MHz, magic angle spinning (MAS) rate of 5 kHz and contact time of 2 ms. All the spectra were collected over 1.5 h (1024 scans).

### 2.9 X-ray diffraction (XRD) analysis

The crystallinity index (Crl) and crystalline structure changes of the samples were investigated by X-ray diffraction (XRD) analysis. The X-ray diffraction (XRD) measurement was performed by means of an X'Pert Pro MPD X-ray diffractometer (Philips-FEI, Netherlands) with Cu K $\alpha$  radiation. The applied current and accelerating voltage were 30 mA and 40 kV, respectively. Diffractograms were collected in the range of  $2\theta=6-60^\circ$  at a scanning rate of  $0.1^\circ \text{ s}^{-1}$ . The crystallinity index (Crl) was calculated according to Eq. (2):

$$\text{Crl} = (I_{002} - I_{\text{am}}) / I_{002} \quad (2)$$

Where  $I_{002}$  is the overall intensity of the peak at  $2\theta$  about  $22^\circ$ , representing the crystalline part of the material, and  $I_{\text{am}}$  is the intensity of the baseline at  $2\theta$  about  $18^\circ$ , representing the amorphous part of the material.<sup>13</sup>

### 2.10 Thermal gravimetric analysis

Thermogravimetric analysis was conducted under a nitrogen atmosphere using a thermal analyzer (NETZSCH STA449F3, Germany). The samples were heated at a temperature interval

of 25-550  $^\circ\text{C}$  at a constant heating rate of 10  $^\circ\text{C min}^{-1}$  and a flow rate of 25  $\text{mL min}^{-1}$ .

## 3. Results and discussion

### 3.1 Effects of reaction conditions on the yield and DS of E-CNC

With the effect of mechanochemistry, esterified cellulose nanocrystals were obtained, in which the nanocrystallization and esterification took place simultaneously. In our early experiment, we have investigated the rotational speed on the yield and characteristics of E-CNC, and found that the effect of rotational speed on the yield and characteristics of E-CNC was less significant. The effects of ball milling time, reaction temperature and ultrasonication time on the yield and degree of substitution (DS) were investigated here. Fig. 2a shows the effect of ball milling time on the yield and DS values, that is, at a reaction temperature of 120  $^\circ\text{C}$ , reaction time of 5 h and ultrasonication time of 3 h, the yield of E-CNC product increases from 17.45% to 43.06% with the ball milling time increasing from 1 h to 2 h. This result arises from the transfer of much more imposed stress produced during ball milling, while the action of ball milling causes the cleavage of intermolecular and intramolecular hydrogen bonds in cellulose chains, which leads to the exposure of more free hydroxyl groups.<sup>14</sup> In addition, the continuous particle refinement and the efficient mixing of acetic acid and cellulose pulp result from ball milling, which promotes sequential esterification. This yield decreases to 34.37% when the ball milling time is extended to 3 h, which may be attributed to the excessive destruction of the crystalline regions during ball milling. The graph shows that DS values increase as the ball milling time increases to 2 h, and then drops to 0.2 as the ball milling time is extended to 3 h. This phenomenon can be explained by the initial acetylation of the disordered accessible regions of the cellulose, followed by esterification at interior regions of the cellulose crystals. As more hydroxyl groups are exposed, only part of them could be acetylated under the experimental conditions.

The effects of reaction temperature on the yield and DS values of E-CNC product are shown in Fig. 2b. With other factors constant, the yield is up to 44.82% at 120  $^\circ\text{C}$  and decreases to 28.84% at 140  $^\circ\text{C}$ , which may be explained by the fact that the reactivity was enhanced with the increase of temperature. However, at higher temperature ( $> 120^\circ\text{C}$ ), the hydrolysis of  $\beta$ -glucosidic bonds of cellulose takes place, followed by an excessive disintegration of cellulose pulp.

Fig. 2c shows the effect of ultrasonication time on the yield and DS values of E-CNC product. With the ultrasonication time varying from 2 h to 3 h and other parameters constant, the yield of E-CNC product increases from 17.81% to 43.21%. This is probably due to the fact that the ultrasonication treatment allows the formation, growth and collapse of cavitation bubble in aqueous solution.<sup>15</sup> The resulting ultrasound energy can be transferred to cellulose chains through the cavitation process, and break down the

interaction forces between cellulose microfibrils, facilitating the disintegration of amorphous regions of cellulose and are

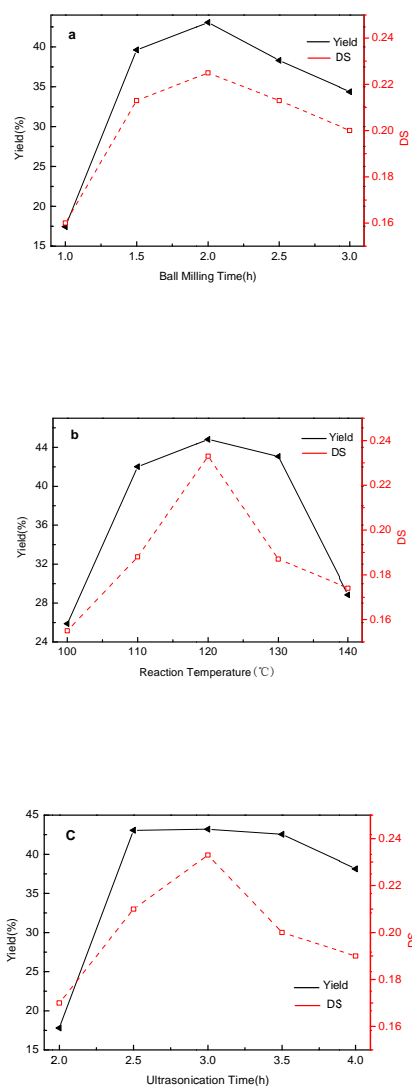


Fig. 2 Effect of (a) ball milling time, (b) reaction temperature and (c) ultrasonication time on the yield and degree of substitution (DS) of E-CNC.

beneficial for the reagent to enter the interior cellulose fibers.<sup>16</sup>

### 3.2 Morphological analysis

The FE-SEM images of cellulose pulp and E-CNC powders are shown in Fig. 3. A curled and flat shape is observed in the SEM image of cellulose pulp (Fig. 3a), and the surface of cellulose pulp is separated into individual micro-sized fibers. In fact, these micro-sized cellulose fibers are composed of strong hydrogen bonding nanocrystals.<sup>17</sup> Under the effects of mechanochemical process, individual nanocrystals could be obtained. It can be seen that the surfaces of cellulose pulp are smooth and clean while the E-CNC are rougher (Fig. 3b), indicating that acetylation has affected the structure of fibers.

As is shown in the TEM micrographs of E-CNC (Fig. 3c, 3d), short rod-like E-CNC are obtained with estimated widths ranging from 20 nm to 40 nm and lengths distributing between 130 nm and 230 nm, which is similar to other studies.<sup>18</sup> These nanocrystals display a classical web-like network structure and occur as very long entangled cellulosic filaments, which could provide higher reinforcing capability for composite applications.<sup>19</sup> Similar result was also found in other literature, which reported that the strong H-bonding among nanocrystals led to the formation of self-assembled networks.<sup>20</sup> In addition, the lower degree of agglomeration of nanocrystals bundles may be due to the replacement of hydroxyl groups in cellulose by acetyl groups, leading to the cellulose to be more hydrophobic and thus resulting in better dispersion.

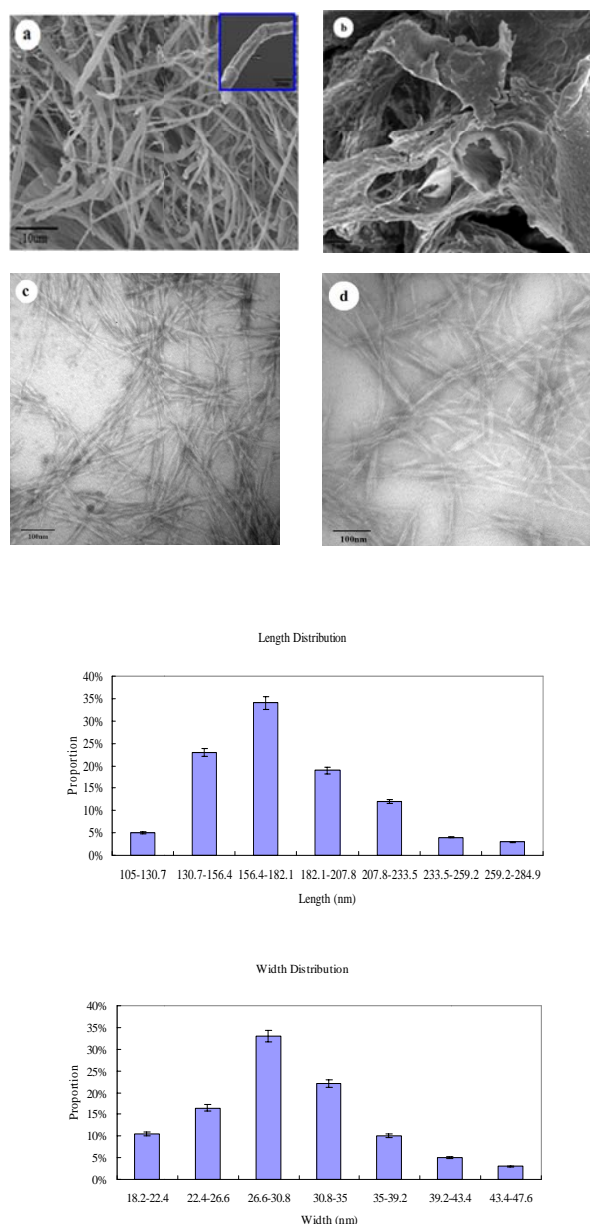


Fig. 3 SEM and TEM images of cellulose pulp and E-CNC, and the length and width distributions of E-CNC.

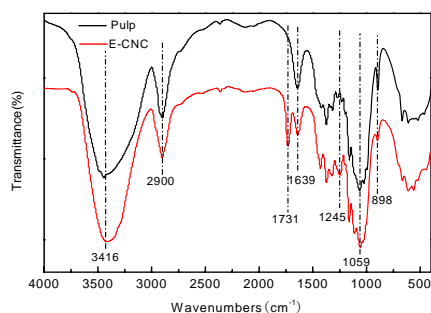


Fig. 4 FTIR spectra of cellulose pulp and E-CNC.

### 3.3 FTIR analysis

Fig. 4 shows the FTIR spectra of cellulose pulp and E-CNC material. In the two spectra, the absorbance at 3416, 2900, 1639, 1059, and 898  $\text{cm}^{-1}$  is associated with native cellulose. The bands at 3416  $\text{cm}^{-1}$  and 2900  $\text{cm}^{-1}$  are assigned to hydrogen bond O-H stretching vibration and the C-H symmetric stretching vibration, respectively. The peak at 1639  $\text{cm}^{-1}$  corresponds to O-H bending of the absorbed water. The absorption band at about 898  $\text{cm}^{-1}$  could be attributed to the asymmetric out of plane ring stretching in cellulose, which is also due to the  $\beta$ -linkage and the amorphous form in cellulose.<sup>21-22</sup> The strong absorption peak at 1059  $\text{cm}^{-1}$  arises from the stretching vibration of C-O bond in cellulose, as well as the C-O bond in hemiacetal of pyranose, which weakens in E-CNC because of the reduction in molecular weight.<sup>23</sup> As for the E-CNC, the peak locating at 1731  $\text{cm}^{-1}$  is attributed to the C=O stretching of carbonyl in the ester bonds.<sup>24</sup> The vibration peak at 1245  $\text{cm}^{-1}$  corresponds to C-O stretching of acetyl group. These two peaks confirm the acetylation of cellulose fibers. In addition, as for the E-CNC, the peak area at 3416  $\text{cm}^{-1}$  is lower than that of cellulose pulp, indicating a partial acetylation. The peak at around 1700  $\text{cm}^{-1}$  is associated with the stretching vibration of free carboxylic group in the acetic acid.<sup>25</sup> The absence of this peak indicates that the product is free of unreacted acetic acid.

### 3.4 XPS characterization

Fig. 5 shows the XPS survey spectra of cellulose pulp and E-CNC material. The low resolution scan model reveals that the primary elements present in the cellulose pulp and E-CNC are C and O, which occur at about 284.5 eV and 533 eV, with no other elements existing in the XPS spectra. Based on the total area of peaks and the respective photoemission cross-sections, the relative distribution of the composition of O and C and the oxygen/carbon [O/C] ratio for cellulose pulp and E-CNC are determined. As for cellulose pulp, the composition of O and C is 41.85% and 58.15%, respectively. By opposite, the composition of O and C for E-CNC is 39.57% and 60.43%, respectively. The O/C ratios are 0.72 for cellulose pulp and 0.65 for E-CNC. The decrease in O/C ratios for E-CNC is

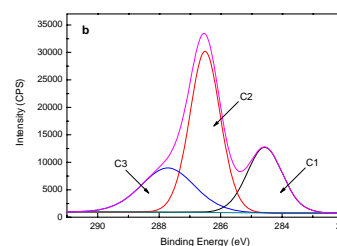
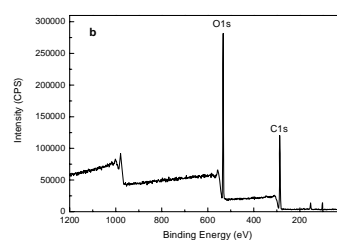
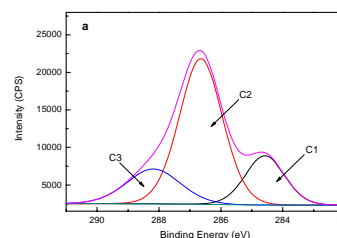
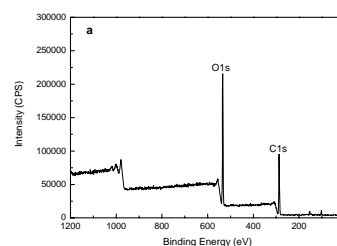


Fig. 5 XPS survey spectra of (a) cellulose pulp and (b) E-CNC.

probably due to the acetylation of cellulose. The high resolution scan of the C1s regions of cellulose pulp and E-CNC are deconvoluted into four peaks that are expressed as C1, C2, C3 and C4, which provide the relative areas of the C1 (C-H, C-O), C2 (C-O), C3 (O-C-O or C=O) and C4 (O-C=O) moieties. As to C4, it is omitted here as it is low in content. The variation of peak area contributions of the C1, C2 and C3 components of cellulose pulp and E-CNC show that C1 and C2 components are the major constituents of C1s in bamboo pulp. The C1 contributions increased from 19.21% to 23.80%, while the contributions of C2 decreased from 62.34% to 52.07%. This

indicates the increase of C-C or C-H components and the decrease of hydroxyl groups in cellulose. The decrease in the O/C ratios and the corresponding increase in the contributions of the C1 following the esterification reactions clearly show the occurrence of the expected surface modification of the cellulose fibers.

### 3.5 Solid-state $^{13}\text{C}$ NMR spectroscopy

Fig. 6 shows the CP-MAS  $^{13}\text{C}$  NMR spectra of unmodified cellulose pulp and E-CNC. The  $^{13}\text{C}$  NMR spectra of all the cellulose samples present the characteristic signals of cellulose. The strong signals in the region between 60 and 120 ppm are assigned mainly to the different carbons of cellulose. The two resonances at 62 and 64.5 ppm are assigned to the disordered and crystalline regions of C6 carbons of cellulose, and the signals between 70 and 75 ppm are assigned to C2, C3 and C5 carbons of the glucopyranose rings in the crystalline regions.<sup>26</sup> The signals at 83.5 and 88.5 ppm are attributed to the disordered and crystalline regions of C4 carbons, respectively. The resonance at 104.5 ppm resulting from the C1 carbons of cellulose structure is ascribed to the crystalline regions of cellulose.<sup>27</sup> The peaks at 88.5 and 64.5 ppm ascribed to the crystalline regions remain the same, which indicates that only a very small part of crystalline region might be altered by the esterification.<sup>28</sup> This hypothesis can be supported by the XRD analysis. After esterification, the characteristic signals of the grafted moieties occur at 174 and 21 ppm, corresponding to the carbons of the carbonyl and methyl groups, respectively. The crystalline structure of cellulose samples can be also investigated by NMR spectroscopy. The crystallinity index can be obtained by evaluating the C4 signal of cellulose, however, the intensity of C4 signal changes little, confirming that the crystalline region of cellulose is not altered.

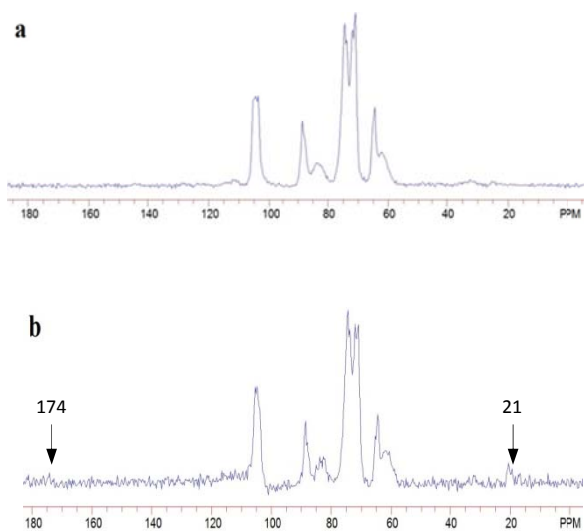


Fig. 6 CP-MAS  $^{13}\text{C}$  NMR spectra of (a) cellulose pulp and (b) E-CNC.

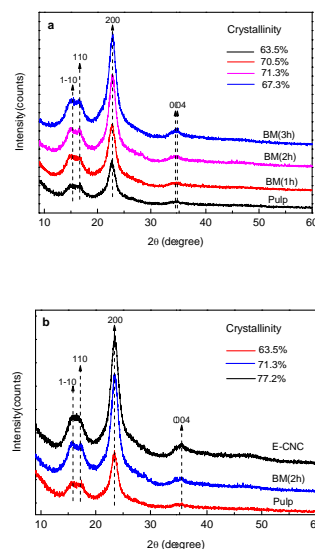


Fig. 7 XRD patterns of untreated and mechanochemical treated cellulose samples. (a) XRD spectra of cellulose pulp and ball milled samples for 1 h, 2 h and 3 h, labeled as BM (1 h), BM (2 h) and BM (3 h), respectively. (b) XRD spectra of cellulose pulp, BM (2 h) and E-CNC.

### 3.6 X-ray diffraction (XRD) analysis

To gain further insights into the crystalline structure changes caused by mechanochemical process, X-ray diffraction (XRD) analysis was conducted. XRD patterns of all the cellulose samples and the calculated crystalline index are shown in Fig. 7. All the samples have similar diffraction patterns with four diffraction peaks at  $2\theta=15.8^\circ$ ,  $17.3^\circ$ ,  $23.5^\circ$  and  $35.4^\circ$ , corresponding to the (1-10), (110), (200) and (004) crystallographic planes, which are in agreement with the characteristic diffraction peaks of cellulose I $\beta$ ,<sup>29</sup> indicating that the crystalline type of cellulose is not altered during the ball milling and ultrasonication treatments in this study. In order to investigate the evolution of crystalline structure of cellulose during the ball milling process, XRD spectra of BM (1 h), BM (2 h) and BM (3 h) are measured and the diffractograms are shown in Fig. 7a. During the ball milling process, the peak intensity of  $23.5^\circ$  increases, confirming the cleavage of glycosidic linkages and the destruction of the hydrogen bond network in cellulose. Compared to cellulose pulp, the crystallinity index of BM (2h) increases from 63.5% to 71.3%. Extending the ball milling time from 2 h to 3 h results in the decrease of the crystallinity index from 71.3% to 67.3%, this is probably due to the excessive destruction of crystalline cellulose.

As is shown in Fig. 7b, the peak intensity of the (200) plane increases after mechanochemical treatments. The calculated crystallinity index (Crl) of cellulose pulp, BM (2 h), and E-CNC are 63.5%, 71.3% and 77.2%, respectively. The increase of the degree of crystallinity for E-CNC, compared to that of cellulose pulp, can be explained by the degradation of amorphous regions and disordered regions of cellulose during mechanochemical treatments. Moreover, the cellulose samples after esterification still maintain high crystallinity index, confirming that the modification occurred essentially

the surface and possibly at the amorphous regions of cellulose.<sup>30</sup> These results are in good agreement with the FTIR results. The crystallinity of cellulose is known as one of the main factors determining its mechanical and thermal properties. Higher crystallinity in E-CNC is associated with higher tensile strength and thermal stability, which is expected to be beneficial for producing high-strength composite materials.

### 3.7 Thermogravimetric analysis (TGA)

Representative TG and DTG curves of cellulose pulp and E-CNC are shown in Fig. 8. Cellulose pulp shows an initial small drop between 25 °C and 120 °C associated with the evaporation of water molecules contained in the sample, which is not obvious for E-CNC. This indicates that the acetylated products are more hydrophobic than native cellulose. For cellulose pulp, the initial thermal decomposition occurs at 286 °C, followed by a drastic reduction in weight between 286 °C and 350 °C. By contrast, the significant weight loss for E-CNC occurs in the range of 315-367 °C, followed by a slow weight loss up to 450 °C. Moreover, the DTG curves (Fig. 8b) show that the thermal decomposition peaks of the maximum weight loss appear at 326 °C for cellulose pulp and 350 °C for E-CNC, which is due to the fact that the thermal decomposition of cellulose. All of the above results indicate that the thermal stability of E-CNC is higher than that of cellulose pulp. The thermal stability of cellulose is affected by crystalline order which increases after the nanocrystallization and acetylation.<sup>31</sup> This explains why the thermal stability of E-CNC is higher than that of cellulose pulp. The high thermal properties of the E-CNC may broaden the fields of application of cellulose fibers, especially at temperature higher than 200 °C for biocomposites processing.

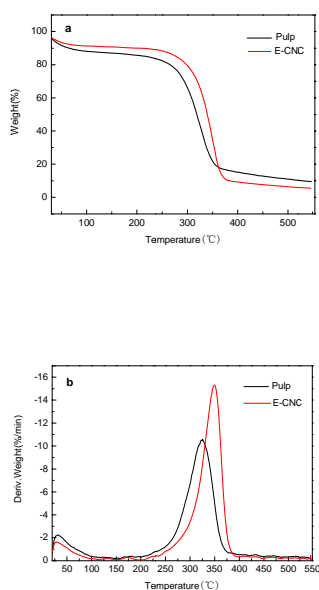


Fig. 8 (a) TG-curves and (b) DTG-curves of cellulose pulp and E-CNC.

## 4. Conclusions

Esterified cellulose nanocrystals (E-CNC) were manufactured via one-pot tandem reactions with the catalysis of DMAP. Ball milling plays an important role as mechanochemical activation during the tandem reactions process. The mechanical shearing and friction forces generated break down the interaction force between cellulose microfibrils, leading to the nanocrystallization and acetylation of cellulose simultaneously. The resulting E-CNC particles are of 130-230 nm in length and 20-40 nm in width, respectively. In addition, the E-CNC have high crystallinity index (77.2%), indicating the maintenance of crystalline region. Therefore, this study provides an efficient approach and mild operating conditions to prepare functionalized cellulose nanocrystals.

## Acknowledgements

We appreciate the generous financial support of the Scientific Research Foundation of Graduate School of Fujian Agriculture and Forestry University (Grant No. 1122yb018), the Project of Advanced Forestry Science and Technology (Grant No. 2014-4-30) and the National Natural Science Foundation of China (Grant No. 31170520, 31370560).

## References

- 1 A. Müller, M. Zink, N. Hessler, F. Wesarg, F. A. Müller, D. Kralisch and D. Fischer, *RSC Adv.*, 2014, **4**, 57173-57184.
- 2 L. C. Tomé, R. J. Pinto, E. Trovatti, C. S. Freire, A. J. Silvestre, C. P. Neto and A. Gandini, *Green Chem.*, 2011, **13**, 419-427.
- 3 S. Ifuku, M. Nogi, K. Abe, K. Handa, F. Nakatsubo and H. Yano, *Biomacromolecules*, 2007, **8**, 1973-1978.
- 4 M. Pešić, C. López, J. López-Santín and G. Álvaro, *Appl. Microbiol. Biotechnol.*, 2013, **97**, 7173-7183.
- 5 A. Bruggink, R. Schoevaart and T. Kieboom, *Org. Process Res. Dev.*, 2003, **7**, 622-640.
- 6 K. Ko, K. Nakano, S. Watanabe, Y. Ichikawa and H. Kotsuki, *Tetrahedron Lett.*, 2009, **50**, 4025-4029.
- 7 H. Hagiwara, H. Inoguchi, M. Fukushima, T. Hoshi and T. Suzuki, *Tetrahedron Lett.*, 2006, **47**, 5371-5373.
- 8 A. Sakakura, K. Kawajiri, T. Ohkubo, Y. Kosugi and K. Ishihara, *J. Am. Chem. Soc.*, 2007, **129**, 14775-14779.
- 9 Z. Liao, Z. Huang, H. Hu, Y. Zhang and Y. Tan, *Bioresour. Technol.*, 2011, **102**, 7953-7958.
- 10 A. Bruckmann, A. Krebs and C. Bolm, *Green Chem.*, 2008, **10**, 1131-1141.
- 11 C. Freire, A. Silvestre, C. P. Neto and R. Rocha, *Cellulose*, 2005, **12**, 449-458.
- 12 D.-Y. Kim, Y. Nishiyama and S. Kuga, *Cellulose*, 2002, **9**, 361-367.
- 13 W. Y. Hamad and T. Q. Hu, *Can. J. Chem. Eng.*, 2010, **88**, 392-402.
- 14 P. Huang, M. Wu, S. Kuga and Y. Huang, *Cellulose*, 2013, **2**, 2175-2178.
- 15 Q. Lu, W. Lin, L. Tang, S. Wang, X. Chen and B. Huang, *J. Mater. Sci.*, 2015, **50**, 611-619.
- 16 P. B. Filson and B. E. Dawson-Andoh, *Bioresour. Technol.*, 2009, **100**, 2259-2264.
- 17 K. Abe and H. Yano, *Cellulose*, 2010, **17**, 271-277.
- 18 M. M. Haafiz, A. Hassan, Z. Zakaria and I. Inuwa, *Carbohydr. Polym.*, 2014, **103**, 119-125.

## ARTICLE

Journal Name

- 19 A. Bhatnagar and M. Sain, *J. Reinf. Plast. Compos.*, 2005, **24**, 1259-1268.
- 20 R. M. Sheltami, I. Abdullah, I. Ahmad, A. Dufresne and H. Kargarzadeh, *Carbohydr. Polym.*, 2012, **88**, 772-779.
- 21 A. Alemdar and M. Sain, *Bioresour. Technol.*, 2008, **99**, 1664-1671.
- 22 J. P. Reddy and J.-W. Rhim, *Carbohydr. Polym.*, 2014, **110**, 480-488.
- 23 X. Sun, F. Xu, R. Sun, P. Fowler and M. Baird, *Carbohydr. Res.*, 2005, **340**, 97-106.
- 24 V. Tserki, N. Zafeiropoulos, F. Simon and C. Panayiotou, *Composites Part A*, 2005, **36**, 1110-1118.
- 25 N. Zafeiropoulos, G. Dijon and C. Baillie, *Composites Part A*, 2007, **38**, 621-628.
- 26 P. Tingaut, T. Zimmermann and F. Lopez-Suevos, *Biomacromolecules*, 2009, **11**, 454-464.
- 27 X. Wang, H. Li, Y. Cao and Q. Tang, *Bioresour. Technol.*, 2011, **102**, 7959-7965.
- 28 K. Zhang, E. Brendler, A. Geissler and S. Fischer, *Polymer*, 2011, **52**, 26-32.
- 29 A. D. French, *Cellulose*, 2014, **21**, 885-896.
- 30 L. Tang, B. Huang, Q. Lu, S. Wang, W. Ou, W. Lin and X. Chen, *Bioresour. Technol.*, 2013, **127**, 100-105.
- 31 J. E. Sealey, G. Samaranyake, J. G. Todd and W. G. Glasser, *J. Polym. Sci., Part B: Polym. Phys.*, 1996, **34**, 1613-1620.

RSC Advances Accepted Manuscript